analytical chemistry

pubs.acs.org/ac Article

Near Infrared-II Photothermal and Colorimetric Synergistic Sensing for Intelligent Onsite Dietary Myrosinase Profiling

Ling Qiao,[§] Wenchao Lang,[§] Caixia Sun, Yining Huang, Ping Wu, Chenxin Cai,* and Bengang Xing*

Cite This: *Anal. Chem.* 2023, 95, 3856−3863 Read Online

ACCESS | Metrics & More | Article Recommendations | Supporting Information

ABSTRACT: Myrosinase (Myr) is a type of critical β-thioglucosidase enzyme activator essential for sustaining many functional foods to perform their health-promoting functions. An accurate and reliable Myr test is meaningful for food quality and dietary nutrition assessments, whereas the currently reported methods do not guarantee specificity and have high reliance on instrumentation, which are not suitable for rapid and onsite Myr screening especially in complex systems from various sources. Herein, we present a unique NIR-II absorption-based photothermal-responsive colorimetric biosensor for anti-interference onsite Myr determination and realization of rapid visualized outputs with the aid of smartphone calculation. Typically, assisted by glucose oxidase (GOx), Myr specifically converts the sinigrin substrate into hydrogen peroxide (H_2O_2) that can oxidize 3,3′,5,5′-tetramethylbenzidine (TMB) catalyzed by AuNPs to form a charge transfer complex (CTC) with NIR-II absorption and photothermal characters. Delightfully, such a proposed method is able to determine Myr within a wide range of 0 to 172.5 mU/mL with a detection limit down to 2.96 mU/mL. Moreover, simple, rapid, and real-time visual Myr identification in actual food-sourced samples could also be readily achieved by smartphone readout processing, with the promising advantages of anti-interference, high accuracy, and low cost as well as labor-saving and intelligence engagement, thus providing great feasibility for precise measurement in complex and dynamic dietary sample analysis. Overall, our proposed method presents a novel technology for onsite dietary Myr enzyme profiling, which is promising to be applied in the food industry for nutritional composition profiles, freshness evaluation, and quality assessment.

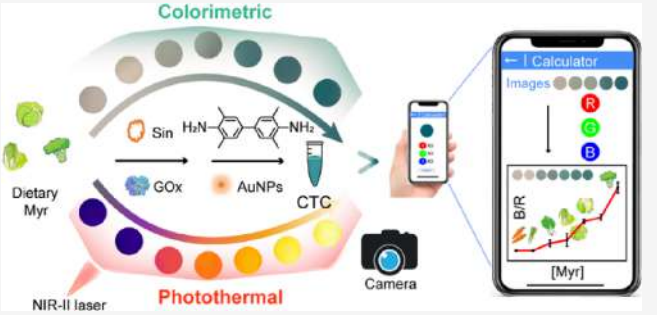

1. INTRODUCTION

There is growing interest in chemoprevention, which is intended to prevent or suppress diseases through the chronic administration of synthetic or natural bioactive agents. Isothiocyanates (ITCs) have been reported to possess wonderful chemopreventive effects, including anti-inflammatory,[1] antioxidant,[2] and antitumor effects,[3] yet they are naturally stored in an inactive form named glucosinolates in crucifers with significant edible and commercial value such as broccoli, cauliflower, watercress, Brussels sprouts, and cabbage.[4,5] Only after activation by an endogenetic β-thioglucosidase enzyme called myrosinase (Myr), these secondary metabolites glucosinolates (Gls) can be converted to ITCs and hydrolysis contributes to not only a special taste but also health benefits to the human body. Studies have suggested that increasing the ingestion of cruciferous vegetables can reduce the incidence of various diseases,[6,7] but the key activator Myr enzyme could be easily denatured through wilting in storage and transporting or food processing[8,9] and therefore significantly hinders the utilization of ITCs through diet. What is more, the Myr content varies across different species under the Cruciferae family and even different parts of vegetables within one species.[10] In order to better exploit the chemopreventive effects of the Gls-Myr-ITCs system and obtain these perishable micronutrient Myr to activate sufficient ITCs, the detection of Myr is crucial for food quality assessments and evaluation of the nutritional compositions and therapeutic effects of functional food.

To the best of our knowledge, the current technology for Myr detection still mainly relies on classical techniques, which include spectrophotometric assay (UV),[11,12] high-performance liquid chromatography (HPLC),[13,14] gas chromatography−mass spectrometry (GC−MS),[15,16] pH-salt assay,[17,18] etc., which work fine. However, the deficiency in specificity and the requirement of sophisticated instrumentation are always the challenging concerns. Some new methods such as immunological methods could detect denatured Myr with no nutritional value and may lead to false-positive signals,[19,20]

Received: December 7, 2022
Accepted: January 30, 2023
Published: February 9, 2023

https://doi.org/10.1021/acs.analchem.2c05474
Anal. Chem. 2023, 95, 3856−3863

and on-gel detection requires extensive gel preparations, which are time-consuming, labor-intensive, and not suitable for onsite Myr tests.[21,22] Consequently, it is highly desired to develop a reliable, simple, interference-free, and rapid method for real-time Myr profiles in complex dietary samples.

To break the hurdles of the aforementioned techniques, nanomaterial-based colorimetric assays have recently attracted academic and industrial attention due to the merits of their simple operation, low cost, easy visualization, and availability for onsite detection.[23−25] Recently, a 3,3′,5,5′-tetramethylbenzidine (TMB)−H_2O_2 colorimetric system has been widely used in bioanalysis and clinical application.[26,27] To further strengthen the applicability of detection, the gold nanoparticles (AuNPs) have become an ideal candidate as an enzyme-mimicking nano-catalyst because of their high stability, easy use, and wider working temperature and pH values than most natural enzymes (e.g., horseradish peroxidase, superoxide dismutase, esterase, etc.), which are more conducive to onsite determination.[28−31] For example, Tang *et al.* developed a self-powered temperature sensor based on Seebeck effect transduction induced by the one-electron oxidation product (ox-TMB) of TMB, which could be applied to α-fetoprotein photothermal-thermoelectric analysis.[32] To further reduce the instrument dependence for point-of-care screening, intelligent portable devices have been employed to achieve instant analysis owing to their capacity for colorimetric data collection and processing.[33,34] For instance, Li *et al.* fabricated a simple sensing platform for enrofloxacin analysis based on the grayscale values of images decomposed by a smartphone application.[35] However, all of these studies used the absorption of CTC at the visible region, which overlaps with chlorophyll, impeding further practical application in detection of plant-derived samples.[36] Fortunately, our group and others recently discovered that CTC formed by the $\pi-\pi$ interaction between diamine (TMB, as donor) and diimine (two-electron oxidation product, $oxTMB^{2+}$, as acceptor) has a high absorption at the second near-infrared window (NIR-II).[37−40] Such unique absorption and photothermal effects at the NIR-II region not only have been widely used in diagnosis and treatment[41,42] but also possess the great potential of low-to-zero background, anti-interference, and rapid readout from a thermometer confronting complex environment for analysis and monitor.[43−45] Also, to the best of our knowledge, an NIR-II-induced, smartphone-assisted photothermal responsive and colorimetric assay has hardly been applied to food analysis and nutrient detection of actual samples of plant origins.

Inspired by the aforementioned perspectives, we explored a novel sensor that combines the photothermal effects and colorimetric signals for rapid and precise onsite Myr analysis at the NIR-II window via smartphone readout (Scheme 1). First, a variety of known concentrations of Myr were mixed with sinigrin (Sin) and GOx to produce a series of solutions containing varying amounts of H_2O_2. Upon addition of TMB and AuNPs to the solution, H_2O_2 would be decomposed to •OH thanks to the catalysis of AuNPs and TMB would be oxidized and transformed into CTC with a blue color and broad absorption from the ultraviolet to NIR-II region.[46] Then, the temperature signals and infrared thermal images would be acquired as a result of CTC absorbance at 1064 nm, which could enhance the detection accuracy. Finally, in order to achieve rapid onsite Myr analysis, we further exploited a smartphone-based intelligent processing system named "Calculator" based on the relationship between the values of the

Scheme 1. Schematic Illustration of Rapid and Simple NIR-II Photothermal Responsive Onsite Myr Detection via Smartphone Readout

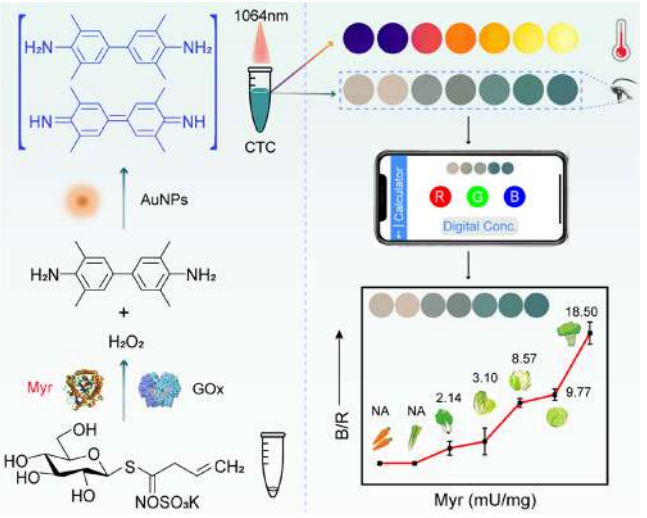

obtained colorimetric or thermal images with the Myr concentrations and successfully applied them for precisely quantitating Myr in real samples including various vegetables, dietary supplements, and commercial wasabi powder. The temperature-responsive and colorimetric sensing platform not only enables rapid qualitative and quantitative Myr onsite analysis via smartphone readout but also shows potential applications in the fields of food quality and nutrition analysis.

2. EXPERIMENTAL SECTION

2.1. Materials and Apparatus. AuNPs were prepared according to previous procedures with minor modifications.[47] Sinigrin (Sin), myrosinase (Myr), horseradish peroxidase (HRP), glucose oxidase (GOx), and a commercial GO detection kit were obtained from Sigma-Aldrich. TMB, H_2O_2 (3%), acetic acid, sodium acetate, KH_2PO_4, KCl, Na_2HPO_4, and NaCl were purchased from Tokyo Chemical Industry Co., Ltd. (Tokyo, Japan). BroccoMax was purchased from Jarrow Formulas (Singapore), and Dualspices Japanese wasabi powder was purchased from iHerb (America), and cruciferous vegetables (broccoli, cauliflower, cabbage, Chinese cabbage, Xiao Bai Cai etc.) and non-cruciferous vegetables (lettuce and carrot) were purchased from the local supermarket. All chemical reagents were of analytical reagent grade and used as received without further treatment. Milli-Q water was used to prepare all solutions. UV−vis−NIR absorption spectra were gauged by a Perkin Elmer Lambda 950 spectrometer, and the micromorphology of prepared AuNPs was characterized by transmission electron microscopy (TEM) on an FEI EM208S TEM (Philips) with an accelerating voltage of 100 kV. Zeta potential was estimated on a Brookhaven 90 Plus nanoparticle size analyzer. Fourier transform infrared spectroscopy (FTIR) was performed on a Bruker Vertex 80v vacuum FTIR spectrometer. The temperature changes and infrared thermal images were obtained by an IR thermal camera (FLIR).

2.2. Photothermal and Colorimetric Assays for Myr Enzyme Detection. A typical spectral photothermal and colorimetric analysis for H_2O_2 and Myr was realized as follows. First, 300 μL of 5 mM TMB, 100 μL of 4.5 nM AuNPs, and 100 μL of H_2O_2 with different concentrations were added into

https://doi.org/10.1021/acs.analchem.2c05474
Anal. Chem. 2023, 95, 3856−3863

500 μL of acetate buffer (pH 4.5), and then the mixture was incubated in a water bath and then cooled to the room temperature for adsorption spectroscopy measurement and photothermal analysis. For Myr detection, Sin (2.5 mM, 30 μL) and GOx (5 mg/mL, 10 μL, according to previous literature[46]) were mixed with different concentrations of Myr first and reacted at 37 °C for 30 min to generate H_2O_2. Then, acetate buffer containing TMB and AuNPs were added into the above solution, incubated at 45 °C for 25 min, and cooled to room temperature, and afterward, the solution was used for the analysis of Myr enzyme activity.

2.3. Detection of Myr in Actual Samples. Myr in dietary supplements and wasabi was detected by the proposed method as follows: 5 mg/mL of broccoli and cabbage vegetables or 10 mg/mL of the rest of the actual samples were heated at 100 °C for 1 h to inactivate Myr; other samples with the same concentration were incubated at room temperature for 30 min, and 90 μL of the samples were mixed with acetate buffer containing GOx (10 μL), TMB (300 μL), and synthesized AuNPs (100 μL) and incubated for another 30 min. For obtaining temperature signals and infrared thermal images, a 1064 nm laser with 1 W/cm^2 was used to irradiate these samples after we collected the absorption spectrum. For Myr analysis in cruciferous plants, we first froze the plant materials using liquid nitrogen for later analysis of Myr.[48] Then, 5 mg of powdered broccoli and cabbage and 10 mg of powdered vegetables were added into 1 mL of PBS buffer depending on the sample and heated at 100 °C for 1 h to inactivate endogenous Myr; then, 60 μL of samples were added into acetate buffer containing exogenous sinigrin, GOx, TMB, and AuNPs, and we collected their absorbance at 1064 nm. Then, the same concentration of samples was incubated at room temperature, and acetate buffer containing sinigrin, GOx, TMB, and AuNPs was mixed with 60 μL of samples. The background signal (A_b) was obtained from the samples treated with 100 °C, and the detection signal (A_d) was collected from the samples treated at room temperature; the amount of Myr was estimated by subtracting A_b from A_d, which gives an increased signal (ΔA) as a result. In addition, the FLIR was used to obtain the temperature signals and infrared thermal images. Considering the relationship between spectra, colorimetric images, temperature signals, and infrared thermal images, we correlated the values of the acquired images with the Myr concentrations via the smartphone-based intelligent processing system "Calculator".[49] Typically, by using "Calculator" with a formula, the obtained experimental images will be resolved into digital pixels presented by red, green, and blue colors (RGB).[50] The ratio of different color intensity values, e.g., blue to red (B/R), will be used to validate Myr amounts in real samples.

3. RESULTS AND DISCUSSION

3.1. Verification of NIR-II Photothermal and Colorimetric Sensing Based on the AuNP-Catalyzed TMB and H_2O_2 System. Before verifying the viability of the AuNP-catalyzed TMB and H_2O_2 system, the morphology and size distribution of the prepared AuNPs were first characterized by transmission electron microscopy (TEM). According to the inset in Figure 1A, the average diameter is approximate ~13 nm, the zeta potential of the solution was measured to be +19.2 mV, and the positive charge on the particles facilitates their dispersion throughout the medium. Figure S1 suggests that AuNPs possessed a strong absorption peak at 527 nm,

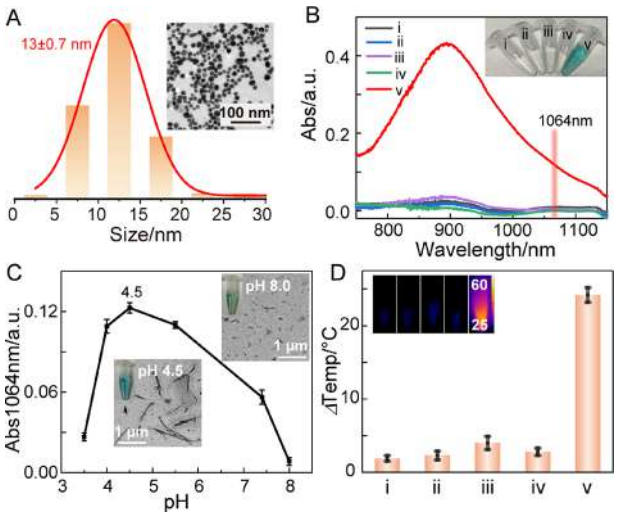

Figure 1. (A) Size distribution of synthesized AuNPs, the top right inset is the TEM image of AuNPs; (B) UV−Vis−NIR spectrum and colorimetric images for H_2O_2 detection; (C) Abs1064nm under different pH values. The lower left inset is the TEM image of CTC at pH 4.5, and the upper right inset is the TEM image at pH 8.0; (D) temperature (ΔTemp) signals and infrared thermal images for H_2O_2 detection, the power density of the 1064 nm laser is 1 W/cm^2. (i) only TMB, (ii) without H_2O_2, (iii) without AuNPs, (iv) without TMB, (v) TMB + H_2O_2 + AuNPs; the final concentrations of H_2O_2, TMB, and AuNPs were 0.25 mM, 1.5 mM, 0.45 nM, respectively.

which is nearly consistent with previous studies.[37] Furthermore, FTIR was employed to obtain absorption bands resulting from the surface functional groups, and Figure S2 depicts that AuNPs possessed a positive charge, the bands at 1650 and 3450 cm^{-1} were assigned to the existence of chitosan, and they represented the amino group and hydroxyl, respectively, which were pivotal for the stability in the aqueous solution.[47] These results demonstrated that the synthesized AuNPs have potential to act as a POD-like enzyme.

In order to illustrate the NIR-II-driven photothermal and colorimetric effect of the AuNPs-TMB-H_2O_2 system, the absorption spectrum of the system with different components was collected, as shown in Figure 1B, and a broad absorption spectrum extending to the NIR-II region emerged (red line) accompanied by a significant color change from colorless to blue (v in the inset) only in the presence of AuNPs, H_2O_2, and TMB. Also, as control, no obvious absorbance and color changes were observed in other situations without the involvement of AuNPs, TMB, or (i)−(iv). Typically, TMB oxidized by H_2O_2 contributes to the assembly of long straight nanobelt structure CTC with a broad absorption spectrum from the UV to NIR-II region,[37,38] as exhibited in Figure S3A and the bottom left inset of Figure 1C. Furthermore, CTC formation was sensitive to changes of pH value with the color changing from blue to green. As shown in Figure 1C and Figure S3B, the absorbance at 1064 nm increased first and then declined with an increase in pH with the most satisfactory result at pH 4.5, and the morphology changed to short nanofragments (top right inset) under higher pH values (e.g., pH = 8.0) due to the generation of yellow diamine as confirmed by our previous studies.[37,38] Then, the samples were irradiated by a 1064 nm laser with a power of 1 W/cm^2 for 5 min, and the FLIR was used to record the temperature changes (Figure 1D); the temperature elevated by 24.2 °C preeminently only when the system contains H_2O_2, AuNPs,

https://doi.org/10.1021/acs.analchem.2c05474
Anal. Chem. 2023, 95, 3856−3863

and TMB, and corresponding infrared thermal images are displayed in inset (v). On the other hand, there was no dramatic temperature rise in the other systems (i–iv) with missing components. These results revealed that the synthesized AuNPs possessed POD-like activity, and the system possessed the ability of NIR-II absorption-driven photothermal and colorimetric sensing for H_2O_2 due to the formation of CTC.

The effect of preparation time on the POD-like activity was examined to obtain AuNPs with the greatest catalytic activity. It can be seen from Figure S4 that the intensity decreased after 30 min; the absorbance at 1064 nm represents the extent of oxidization from TMB to CTC and the POD-like ability of AuNPs. Thus, the activity drops when the time exceeds 30 min due to the aggregation of AuNPs at high temperature over time. Therefore, 30 min was selected as the optimal preparation time for AuNPs. Figure S5A demonstrates that the absorbance at 1064 nm increased as the mole concentration of AuNPs increased from 0.025 to 0.9 nM, and the inset of Figure S5B displays that the color of the solution deepened as the mole concentration of AuNPs increased; we chose 0.45 nM as the optimal concentration of AuNPs in the following steps.

In this system, TMB was used to produce the photothermal agent CTC, so it is vital to optimize the TMB concentration. As shown in Figure S6A, the absorbances at 1064 nm increased in the concentration range of 0.5 to 1.5 mM and decreased at higher concentrations. Figure S6B indicates that the yields of CTC improved with increasing substrate concentrations, reaching a maximum at 1.5 mM TMB concentration. While TMB levels were in excess, a slight color fading was observed, which may be attributed to the formation of $oxTMB^{2+}$ with a light-yellow hue as a result of further oxidation.[51] Therefore, 1.5 mM was the optimal TMB concentration in our system. Then, we also investigated the impact of temperature on the activity of AuNPs, where Figure S7A,B demonstrates that the absorbance at 1064 nm increased with the increase of temperature within the range of 20 to 45 °C and then decreased from 45 to 80 °C; thus, 45 °C was chosen for the following experiments. It is worth noting that the AuNPs retain peroxidase activity even when heated to 80 °C. This is superior to the natural HRP enzyme that loses activity once the temperature exceeds 50 °C.[52] This may be due to the external polymer chitosan being more resistant to high temperatures than small molecules. After optimizing all conditions, their ability to detect commercial H_2O_2 was first evaluated, and the results in Figure S8A, B illustrated that the system could detect H_2O_2 from 1 μM to 2.5 mM with a limit of detection (LOD) of 0.68 μM, comparable to the results published previously.[28]

3.2. Photothermal and Colorimetric Bioassay for Myr Measurement. Next, we investigated the feasibility of this method for Myr tests followed by the optimization of conditions, and the results are shown in Figure 2A. There are no significant changes both in absorption spectrum and images of samples (i–v, containing incomplete component), whereas an obvious absorbance at 1064 nm emerged in sample vi (including all components) accompanied by a vivid color change from colorless to blue. In agreement with the aforementioned results, H_2O_2 only emerged in the presence of Myr and GOx and then interacted with TMB under the catalysis of AuNPs to yield blue CTC with NIR-II absorption. After all samples were treated with a 1064 nm laser, a drastic temperature improvement of nearly 22.5 °C and remarkable

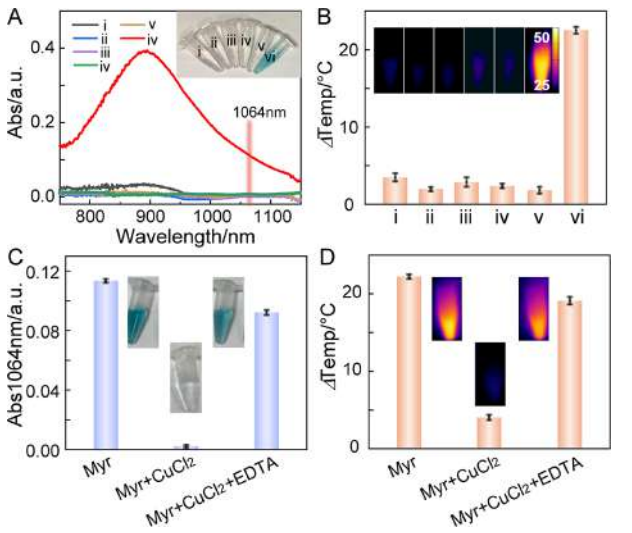

Figure 2. (A) UV–Vis–NIR spectra and colorimetric images and (B) ΔTemp signals and infrared thermal images for Myr detection (i) without AuNPs, (ii) without GOx, (iii) without Myr, (iv) without Sin, (v) without TMB, and (vi) with Sin + Myr + GOx + TMB + AuNPs. The final concentrations of Sin, Myr, GOx, TMB, AuNPs were 0.75 mM, 0.75 mg/mL, 0.5 mg/mL, 1.5 mM, and 0.45 nM, respectively. The power density of the 1064 nm laser is 1 W/cm^2; (C) absorbance at 1064 nm of the Myr test system with Cu^{2+} and EDTA, inset shows the colorimetric images; (D) ΔTemp signals after being irradiated by a 1064 nm laser at 1 W/cm^2 for 5 min, inset is the infrared thermal images.

infrared thermal image was acquired in sample vi (Figure 2B) thanks to the excellent photothermal conversion performance of CTC. In contrast, mild temperature fluctuations and negligible images were observed in other samples (i–v). These results suggested that photothermal and colorimetric signals were only derived from the formation of CTC. Moreover, the viability of analyzing Myr was further studied, and the results of Figure S9 and Figure 2C indicated that absorbance at 1064 nm declined dramatically after Cu^{2+} was added into the system containing Sin, Myr, GOx, TMB, and AuNPs. However, the intensity recovered significantly after adding EDTA into the system, which could combine with Cu^{2+} and diminish the inhibitory effect of Cu^{2+}. The corresponding temperature signals and infrared thermal images are shown in Figure 2D. Similarly, the increase of temperature notably reduced from 22.1 °C to 3.9 °C and then rose to 19 °C, and the infrared thermal images were also altered clearly. All of these results reconfirmed the feasibility of NIR-II absorption-driven photothermal and colorimetric sensing techniques and indicated their potential to analyze Myr in actual samples by exploiting the NIR-II absorption characteristic of CTC.

3.3. Quantitative Analysis of the NIR-II Absorption-Driven Photothermal and Colorimetric Sensing for Myr. After optimizing all conditions, we applied this method to test Myr; however, previous studies indicated that a high Gls concentration has a significant inhibitory effect on Myr activity.[52] Before testing different Myr concentrations, it is necessary to determine the maximum Sin concentration that can be applied. Figure S10A,B illustrates that when the concentration of Sin exceeds 0.75 mM, the working efficiency decreases and the blue color becomes faint because excess Sin binds to the active regulatory sites of Myr. As a result, 0.75 mM was selected as the maximum Sin concentration for

https://doi.org/10.1021/acs.analchem.2c05474
Anal. Chem. 2023, 95, 3856–3863

detecting commercial Myr at varying concentrations and constructing a standard curve. As Figure 3A,B and Figure S11

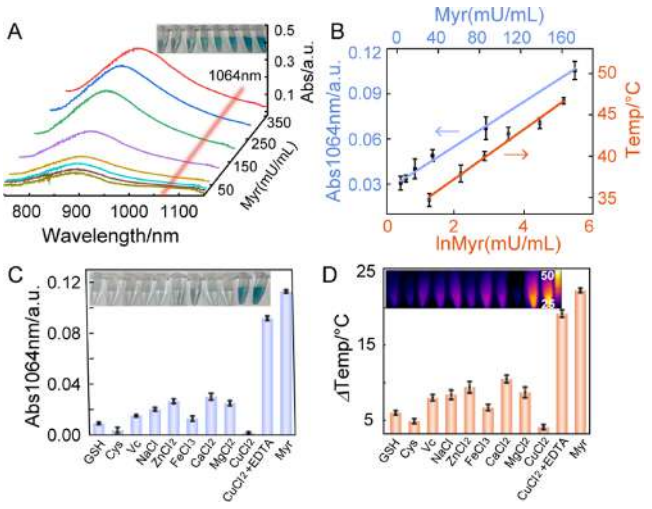

Figure 3. (A) Absorption spectrum of different concentrations of Myr, the corresponding colorimetric image is exhibited in the top right; (B) linear relationship between Abs1064nm and Myr enzyme within the range of 0−172.5 mU/mL (blue) and relationship between temperature and logarithm of Myr enzyme concentration (orange); (C) absorbance at 1064 nm of Myr and various interfering substances, inset shows the colorimetric images; (D) ΔTemp signals after being irradiated by a 1064 nm laser at 1 W/cm^2 for 5 min, and infrared thermal images.

show, when Sin was present at a concentration of 0.75 mM, Myr was detectable in the range of 0−345 mU/mL, and its linear detection range in the absorption spectrum was 0 to 172.5 mU/mL with an LOD of 2.96 mU/mL. Comparatively, our method shows superiority in sensitivity with an LOD lower than that of previously reported work.[18,22] Additionally, the linear relationship between temperature and the logarithm of Myr concentration was also exhibited by the orange line in Figure 3B with a similar trend as indicated previously.[53] These results further validate that the method could be employed to Myr analysis in real samples by both temperature and absorbance variations.

More importantly, such a simple and rapid method gets rid of complicated sample preparation and measurement processing, therefore providing huge potential for onsite detection.

Moreover, specificity is also an important indicator for evaluating the practicability of an analytical technique, so various interfering factors including amino acids, small molecules, and metal ions were also measured by the NIR-II-driven photothermal and colorimetric sensing platform. As exhibited in Figure 3C, the absorbance at 1064 nm of Myr was notably higher than those of other interfering molecules, and a remarkable color change was observed only for Myr, with the absorption spectrum depicted in Figure S12. Additionally, Figure 3D displays the corresponding temperature signals and infrared thermal images, indicating that the temperature elevation of Myr was more apparent than that of other interfering factors after irradiation by a 1064 nm laser. The results implied that the method shows good specificity for the Myr test in a complex matrix environment and potential capacity for the onsite Myr test.

Next, the temperature response to different concentrations of Myr and thermal cycling stability were discussed, as mentioned above; under the catalysis of AuNPs, TMB reacted with H_2O_2 to produce a blue CTC with a broad absorption peak in the NIR-II region. Taking advantage of the property, the samples were irradiated with a 1064 nm laser to obtain the temperature response of different Myr concentrations, as displayed in Figure 4A, and we can quantitatively analyze Myr

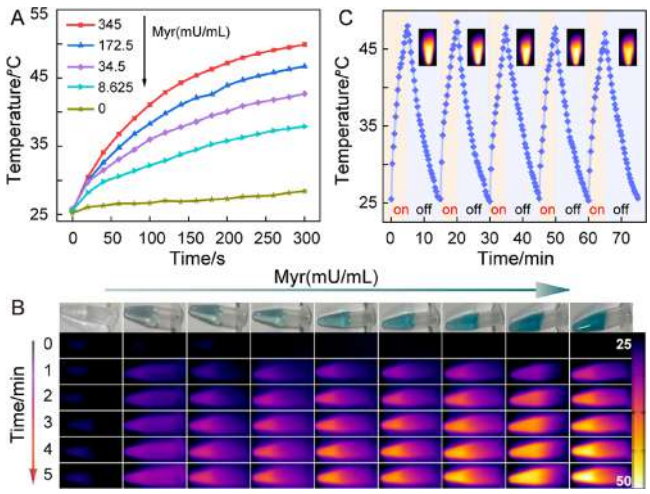

Figure 4. (A) Temperature responses with increasing concentrations of Myr within 5 min and (B) the corresponding infrared thermal image at a different time under 1064 nm laser irradiation with a power of 1 W/cm^2; (C) thermal cycle stability of the Sin + Myr + GOx + TMB + AuNPs system.

by temperature, for example, the temperature corresponding to 345 mU/mL Myr is approximately 49.8 °C. In addition, the corresponding infrared thermal images were captured (Figure 4B). We also evaluated the thermal cycling stability for detecting Myr; as Figure 4C demonstrated, the method still has a good photothermal response even after 5 cycles of laser irradiation. This denotes that the method proposed in this work could be utilized for Myr testing with pleasing thermal stability.

3.4. Intelligent Onsite Determination of Myr in Actual Samples via a Smartphone. We planned to examine the feasibility of accurate analysis in the sophisticated and dynamic system. Toward this purpose, we applied the method to test Myr in actual samples, and we selected some cruciferous and non-cruciferous vegetables, and the dietary supplements BroccoMax and Dualspices Japanese wasabi powder as the detecting samples. For the determination of total Myr in vegetables, all samples were flash-frozen in liquid nitrogen, and in order to avoid the interference of the sample itself, we inactivated the sample at 100 °C for 1 h to ensure the inactivation of Myr. Then, the Myr content in the samples treated at room temperature and high temperature was determined using the method proposed in this work. As demonstrated in Figure S13A, the absorption spectra were obtained by subtracting the absorption spectrum of the samples at high temperature (A_b) from the absorption spectrum of the samples at room temperature (A_d), named ΔAbsorbance (ΔAbs) spectra. Figure 5A shows the ΔAbs at 1064 nm of various vegetables including broccoli, cauliflower, green cabbage, Chinese cabbage, Xiao Bai Cai, lettuce, and carrot. Among them, broccoli has the maximum ΔAbs1064nm value followed by green cabbage, and carrot has the minimum value. Then, their temperature change (Figure S13B) and

https://doi.org/10.1021/acs.analchem.2c05474
Anal. Chem. 2023, 95, 3856−3863

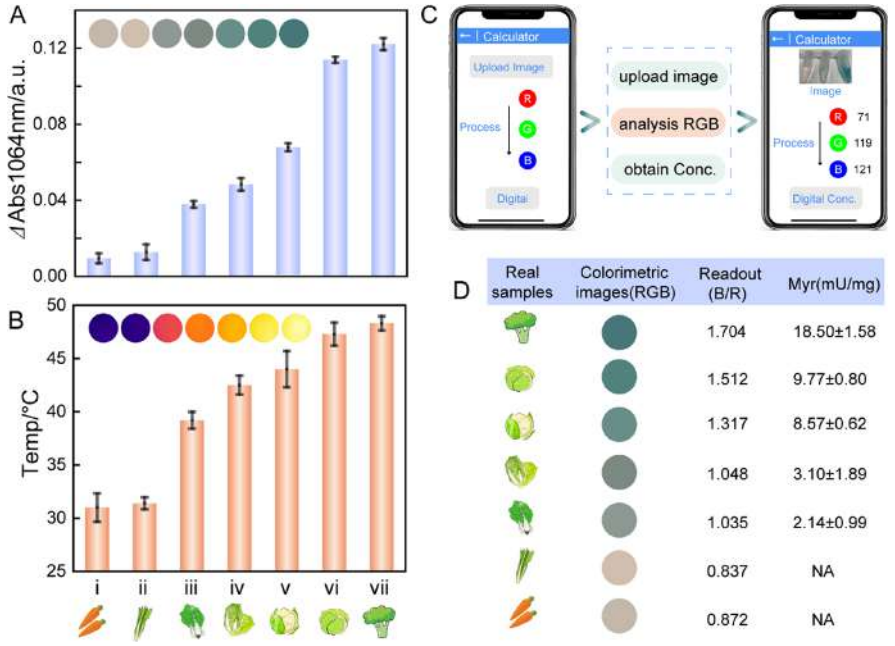

Figure 5. (A) ΔAbs of some vegetables at 1064 nm, inset shows the colorimetric images; (B) Temperature of several vegetables after being irradiated by a 1064 nm laser at 1 W/cm^2 for 5 min, inset is the infrared thermal images. (C) Diagram of Myr enzyme determination by Calculator; (D) B/R value and Myr concentration in actual vegetable samples after being processed by Calculator. Carrot, lettuce, Xiao Bai Cai, Chinese cabbage, cauliflower, green cabbage, and broccoli are represented by the numerals i, ii, iii, iv, v, vi, and vii, respectively.

infrared thermal images (Figure 5B) were also acquired by the FLIR. Based on the established calibration curves, the amounts of Myr per mg of actual samples are listed in Tables S1 and S2, obtained from Abs1064nm and temperature in Figure 5 and Figure S14, respectively. For accurate intelligent onsite Myr analysis, the processing system "Calculator", which involves a conversion formula, was introduced to on-site examine Myr intelligently. The image analysis and processing flowchart of "Calculator" is illustrated in Figure S15, and screenshots of "Calculator" are exhibited in Figure S16. The B/R values were used as a parameter from graphical visualization for quantifying real samples. After uploading and decomposing colorimetric images using "Calculator", the Myr contents in vegetables were obtained via smartphone readout (Figure 5C). The B/R values and corresponding Myr concentrations are exhibited in Figure 5D. The highest Myr content was found in broccoli, which measured to be 18.50 ± 1.58 mU/mg, whereas the Myr contents in lettuce and carrot were below zero, indicating that these non-cruciferous vegetables contained no Myr. Similarly, the Myr concentrations calculated from temperatures corresponding to infrared thermal images follow a consistent trend, indicated in Table S2, which further validated the capability of synergistically screening through NIR-II-activating photothermal and colorimetric signals.

In addition, as shown in Figure S17A,B, the absorption spectrum and temperature change of the dietary supplement and wasabi powder were also acquired. The results in Table S3 reflected that the Myr amount in wasabi powder is much higher than dietary supplement BroccoMax. Further, the Myr content was determined with the aid of "Calculator", and according to the results of Figure S17C,D, the Myr content in 1 mg BroccoMax is about 8.88 ± 0.26 mU, whereas the Myr concentration in 1 mg of wasabi powder is approximately 19.84 ± 0.27 mU, reaffirming the fact that the amount of Myr in wasabi powder is greater than in BroccoMax. All of these results ascertain that the smartphone-based NIR-II absorption-driven photothermal and colorimetric sensing platform exhibits satisfactory performance for the intelligent, convenient, and interference-free detection of Myr in actual samples.

4. CONCLUSIONS

In summary, this work presented a new method for rapid and interference-free detection of Myr based on the NIR-II absorption-driven photothermal and colorimetric synergistic sensing system. The method possesses some forte as below: (i) The usage of NIR-II absorbance at 1064 nm could largely exclude the interference caused by impurities and chlorophyll in plant samples, making it more appropriate for the analysis of Myr in real plant samples. (ii) Temperature signals and near-infrared thermal images generated by the photothermal effect of CTC could further improve the credibility of detection, which makes the results more reliable. (iii) With the assistance of smartphone readout, the colorimetric images could be processed by the intelligent processing system "Calculator" to obtain their RGB values, which are relevant to Myr concentrations, and thus achieve simple and rapid onsite Myr detection from complex and dynamic analytes with favorable results. We believe that such a NIR-II absorption-driven photothermal and colorimetric-based sensing platform will provide a new technology for the intelligent and precise onsite detection of Myr and open a new horizon for food quality assessments and nutritional composition profiles that can benefit the relevant research fields in the future.

■ ASSOCIATED CONTENT

Supporting Information

The Supporting Information is available free of charge at https://pubs.acs.org/doi/10.1021/acs.analchem.2c05474.

Additional experimental details, results, characterization of AuNPs, absorption spectrum, FTIR spectrum and

https://doi.org/10.1021/acs.analchem.2c05474
Anal. Chem. 2023, 95, 3856−3863

zeta potential; optimization of detection conditions, AuNP preparation time, TMB concentration, working temperature; absorption spectrum of the test system with different concentrations of H_2O_2 and Sin and addition of inhibitor and potential interference; illustration and data of smartphone readout from real sample analysis (PDF)

AUTHOR INFORMATION

Corresponding Authors

Chenxin Cai − *Jiangsu Key Laboratory of New Power Batteries, Jiangsu Collaborative Innovation Center of Biomedical Functional Materials, College of Chemistry and Materials Science, Nanjing Normal University, Nanjing 210023, P. R. China*; Email: cxcai@njnu.edu.cn

Bengang Xing − *School of Chemistry, Chemical Engineering & Biotechnology, Nanyang Technological University, Singapore 637371, Singapore*; orcid.org/0000-0002-8391-1234; Email: Bengang@ntu.edu.sg

Authors

Ling Qiao − *School of Chemistry, Chemical Engineering & Biotechnology, Nanyang Technological University, Singapore 637371, Singapore; Jiangsu Key Laboratory of New Power Batteries, Jiangsu Collaborative Innovation Center of Biomedical Functional Materials, College of Chemistry and Materials Science, Nanjing Normal University, Nanjing 210023, P. R. China*

Wenchao Lang − *School of Chemistry, Chemical Engineering & Biotechnology, Nanyang Technological University, Singapore 637371, Singapore*

Caixia Sun − *School of Chemistry, Chemical Engineering & Biotechnology, Nanyang Technological University, Singapore 637371, Singapore*

Yining Huang − *School of Chemistry, Chemical Engineering & Biotechnology, Nanyang Technological University, Singapore 637371, Singapore*

Ping Wu − *Jiangsu Key Laboratory of New Power Batteries, Jiangsu Collaborative Innovation Center of Biomedical Functional Materials, College of Chemistry and Materials Science, Nanjing Normal University, Nanjing 210023, P. R. China*

Complete contact information is available at: https://pubs.acs.org/10.1021/acs.analchem.2c05474

Author Contributions

[§]L.Q. and W.L. contributed equally to this work. All authors have given approval to the final version of the manuscript.

Notes

The authors declare no competing financial interest.

ACKNOWLEDGMENTS

This work is supported by MOE Tier 1 RG4/22, RG6/20, A*Star SERC A1983c0028, A20E5c0090, awarded at Nanyang Technological University (NTU), and the National Natural Science Foundation of China (NSFC) (No. 51929201). L.Q. gratefully acknowledges financial support from the China Scholarship Council (NO.202006860052) and the Postgraduate Research & Practice Innovation Program of Jiangsu Province (KYCX21-1327).

REFERENCES

(1) Townsend, B. E.; Johnson, R. W. *Exp. Gerontol.* **2016**, *73*, 42−48.
(2) De Figueiredo, S. M.; Binda, N. S.; Nogueira-Machado, J. A.; Vieira-Filho, S. A.; Caligiorne, R. B. *Recent Pat. Endocr., Metab. Immune Drug Discovery* **2015**, *9*, 24−39.
(3) Bao, C.; Ko, J.; Park, H.-C.; Kim, M. C.; Kim, J.; Auh, J.-H.; Lee, H. J. *Food Sci. Biotechnol.* **2015**, *24*, 347−351.
(4) Mays, J. R.; Weller Roska, R. L.; Sarfaraz, S.; Mukhtar, H.; Rajski, S. R. *ChemBioChem* **2008**, *9*, 729−747.
(5) Dinkova-Kostova, A. T.; Kostov, R. V. *Trends Mol. Med.* **2012**, *18*, 337−347.
(6) Vainio, H.; Weiderpass, E. *Nutr. Cancer* **2006**, *54*, 111−142.
(7) Kwiatkowska, E.; Bawa, S. *Rocz. Panstw. Zakl. Hig.* **2007**, *58*, 7−13.
(8) Van Eylen, D.; Oey, I.; Hendrickx, M.; Van Loey, A. *J. Agric. Food Chem.* **2007**, *55*, 2163−2170.
(9) Baenas, N.; Marhuenda, J.; García-Viguera, C.; Zafrill, P.; Moreno, D. *Foods* **2019**, *8*, 257.
(10) Piekarska, A.; Kusznierewicz, B.; Meller, M.; Dziedziul, K.; Namieśnik, J.; Bartoszek, A. *Ind. Crops Prod.* **2013**, *50*, 58−67.
(11) Palmieri, S.; Leoni, O.; Iori, R. *Anal. Biochem.* **1982**, *123*, 320−324.
(12) Bellostas, N.; Petersen, I. L.; Sørensen, J. C.; Sørensen, H. *Methods* **2008**, *70*, 918−925.
(13) Kleinwachter, M.; Selmar, D. *J. Biochem. Biophys. Methods* **2004**, *59*, 253−265.
(14) Bonechi, C.; Donati, A.; Tamasi, G.; Pardini, A.; Rostom, H.; Leone, G.; Lamponi, S.; Consumi, M.; Magnani, A.; Rossi, C. *Biophys. Chem.* **2019**, *246*, 25−34.
(15) Lambrix, V.; Reichelt, M.; Mitchell-Olds, T.; Kliebenstein, D. J.; Gershenzon, J. *Plant Cell* **2001**, *13*, 2793−2807.
(16) Wittstock, U.; Agerbirk, N.; Stauber, E. J.; Olsen, C. E.; Hippler, M.; Mitchell-Olds, T.; Gershenzon, J.; Vogel, H. *Proc. Natl. Acad. Sci. U. S. A.* **2004**, *101*, 4859−4864.
(17) Palmieri, S.; Iori, R.; Leoni, O. *J. Agrie. Food Chem.* **1987**, *35*, 617−621.
(18) Finiguerra, M. G.; Iori, R.; Palmieri, S. *J. Agric. Food Chem.* **2001**, *49*, 840−845.
(19) Bones, A. M.; Thangstad, O. P.; Haugen, O. A.; Espevik, T. *J. Exp. Bot.* **1991**, *42*, 1541−1550.
(20) Andréasson, E.; Jørgensen, L. B.; Höglund, A.-S.; Rask, L.; Meijer, J. *Plant Physiol.* **2001**, *127*, 1750−1763.
(21) Sharma, A.; Yogavel, M.; Sharma, A. *J. Struct. Funct. Genomics* **2012**, *13*, 135−143.
(22) Gonda, S.; Szücs, Z.; Plaszkó, T.; Cziáky, Z.; Kiss-Szikszai, A.; Vasas, G.; M-Hamvas, M. *Molecules* **2018**, *23*, 2204.
(23) Jang, J. W.; Kim, H.; Kim, I.; Lee, S. W.; Jung, H. G.; Hwang, K. S.; Lee, J. H.; Lee, G.; Lee, D.; Yoon, D. S. *Anal. Chem.* **2022**, *94*, 6473−6481.
(24) Xu, W.; Jiao, L.; Yan, H.; Wu, Y.; Chen, L.; Gu, W.; Du, D.; Lin, Y.; Zhu, C. *ACS Appl. Mater. Interfaces* **2019**, *11*, 22096−22101.
(25) Wang, X.; Qin, L.; Lin, M.; Xing, H.; Wei, H. *Anal. Chem.* **2019**, *91*, 10648−10656.
(26) Yi, D.; Wei, Z.; Zheng, W.; Pan, Y.; Long, Y.; Zheng, H. *Sens. Actuators, B* **2020**, *323*, 128691.
(27) Liu, X.; Zhang, M.; Chen, Z.; Cui, J.; Yang, L.; Lu, Z.; Qi, F.; Wang, H. *Front. Bioeng. Biotechnol.* **2021**, *9*, 799370.
(28) Jiang, T.; Liu, R.; Huang, X.; Feng, H.; Teo, W.; Xing, B. *Chem. Commun.* **2009**, *15*, 1972−1974.
(29) Liu, R.; Liew, R.; Zhou, J.; Xing, B. *Angew. Chem., Int. Ed.* **2007**, *46*, 8799−8803.
(30) Wang, L. L.; Qiao, J.; Liu, H. H.; Hao, J.; Qi, L.; Zhou, X. P.; Li, D.; Nie, Z. X.; Mao, L. Q. *Anal. Chem.* **2014**, *86*, 9758−9764.
(31) Zhou, W.; Sun, J.; Li, X. *Anal. Chem.* **2020**, *92*, 14830−14837.
(32) Huang, L.; Chen, J.; Yu, Z.; Tang, D. *Anal. Chem.* **2020**, *92*, 2809−2814.
(33) Wang, H.; Yang, L.; Chu, S.; Liu, B.; Zhang, Q.; Zou, L.; Yu, S.; Jiang, C. *Anal. Chem.* **2019**, *91*, 9292−9299.

(34) Zhang, Y.; Zhu, X.; Li, M.; Liu, H.; Sun, B. *J. Agric. Food Chem.* **2022**, *70*, 6059−6071.
(35) Li, D.; Huang, M.; Shi, Z.; Huang, L.; Jin, J.; Jiang, C.; Yu, W.; Guo, Z.; Wang, J. *Anal. Chem.* **2022**, *94*, 2996−3004.
(36) Fossey, A.; Mathura, S.; Beck-Pay, S. L. *Southern Forests* **2009**, *71*, 59−62.
(37) Wang, Z.; Upputuri, P. K.; Zhen, X.; Zhang, R.; Jiang, Y.; Ai, X.; Zhang, Z.; Hu, M.; Meng, Z.; Lu, Y.; Zheng, Y.; Pu, K.; Pramanik, M.; Xing, B. *Nano Res.* **2019**, *12*, 49−55.
(38) Wang, Z.; Zhen, X.; Upputuri, P. K.; Jiang, Y.; Lau, J.; Pramanik, M.; Pu, K.; Xing, B. *ACS Nano* **2019**, *13*, 5816−5825.
(39) Ma, Z.; Foda, M. F.; Liang, H.; Zhao, Y.; Han, H. *Adv. Funct. Mater.* **2021**, *31*, 2103765.
(40) He, X.; Hao, Y.; Chu, B.; Yang, Y.; Sun, A.; Shi, K.; Yang, C.; Zhou, K.; Qu, Y.; Li, H.; Qian, Z. *Nano Today* **2021**, *39*, 101174.
(41) Chen, H.; Shou, K.; Chen, S.; Qu, C.; Wang, Z.; Jiang, L.; Zhu, M.; Ding, B.; Qian, K.; Ji, A.; Lou, H.; Tong, L.; Hsu, A.; Wang, Y.; Felsher, D. W.; Hu, Z.; Tian, J.; Cheng, Z. *Adv. Mater.* **2021**, *33*, 2006902.
(42) Chen, T.; Hou, P.; Zhang, Y.; Ao, R.; Su, L.; Jiang, Y.; Zhang, Y.; Cai, H.; Wang, J.; Chen, Q.; Song, J.; Lin, L.; Yang, H.; Chen, X. *Angew. Chem.* **2021**, *60*, 15006−15012.
(43) Zheng, A.; Liu, H.; Gao, X.; Xu, K.; Tang, B. *Anal. Chem.* **2021**, *93*, 9244−9249.
(44) Li, D.; Qu, C.; Liu, Q.; Wu, Y.; Hu, X.; Qian, K.; Chang, B.; He, S.; Yuan, Y.; Li, Y.; Ko, T.; Yu, A.; Cheng, Z. *Adv. Funct. Mater.* **2020**, *30*, 1906343.
(45) Cong, T. D.; Wang, Z.; Hu, M.; Han, Q.; Xing, B. *ACS Nano* **2020**, *14*, 5836−5844.
(46) Jiang, C.; Zhu, J.; Li, Z.; Luo, J.; Wang, J.; Sun, Y. *RSC Adv.* **2017**, *7*, 44463−44469.
(47) Wu, L.; Shi, C.; Tian, L.; Zhu, J. *J. Phys. Chem. C* **2007**, *112*, 319−323.
(48) Keck, A. S.; Qiao, Q.; Jeffery, E. H. *J. Agric. Food Chem.* **2003**, *51*, 3320−3327.
(49) https://calculator-39f49.firebaseapp.com/#/
(50) Stefan, L.; Denat, F.; Monchaud, D. *Nucleic Acids Res.* **2012**, *40*, 8759−8772.
(51) Gao, L.; Zhuang, J.; Nie, L.; Zhang, J.; Zhang, Y.; Gu, N.; Wang, T.; Feng, J.; Yang, D.; Perrett, S.; Yan, X. *Nat. Nanotechnol.* **2007**, *2*, 577−583.
(52) Pardini, A.; Tamasi, G.; De Rocco, F.; Bonechi, C.; Consumi, M.; Leone, G.; Magnani, A.; Rossi, C. *Food Chem.* **2021**, *355*, 129634.
(53) Fu, G.; Sanjay, S. T.; Zhou, W.; Brekken, R. A.; Kirken, R. A.; Li, X. *Anal. Chem.* **2018**, *90*, 5930−5937.

https://doi.org/10.1021/acs.analchem.2c05474
Anal. Chem. 2023, 95, 3856−3863